

In-situ mid-circuit qubit measurement and reset in a single-species trapped-ion quantum computing system

Yichao Yu,* Keqin Yan, Debopriyo Biswas, Vivian Ni Zhang, Bahaa Harraz, Crystal Noel, Christopher Monroe, and Alexander Kozhanov

*Duke Quantum Center, Department of Electrical and Computer Engineering and Department of Physics
Duke University, Durham, NC 27708*

(Dated: April 24, 2025)

We implement in-situ mid-circuit measurement and reset (MCMR) operations on a trapped-ion quantum computing system by using metastable qubit states in $^{171}\text{Yb}^+$ ions. We introduce and compare two methods for isolating data qubits from measured qubits: one shelves the data qubit into the metastable state and the other drives the measured qubit to the metastable state without disturbing the other qubits. We experimentally demonstrate both methods on a crystal of two $^{171}\text{Yb}^+$ ions using both the $S_{1/2}$ ground state hyperfine clock qubit and the $S_{1/2}$ - $D_{3/2}$ optical qubit. These MCMR methods result in errors on the data qubit of about 2% without degrading the measurement fidelity. With straightforward reductions in laser noise, these errors can be suppressed to less than 0.1%. The demonstrated method allows MCMR to be performed in a single-species ion chain without shuttling or additional qubit-addressing optics, greatly simplifying the architecture.

I. INTRODUCTION

Applications of quantum information science, from computing and simulation [1, 2] to communication [3] and sensing [4], are predicated upon high-fidelity initialization and measurement of quantum systems such as qubits. With increasing demand for interaction complexity and fidelity, classical feedback has become a critical tool for quantum control, with prime examples of auxiliary quantum sensing [5] and quantum error correction [6]. This approach usually requires measurements on a subsystem of auxiliary qubits while not affecting the coherence of the remaining data qubits.

In atomic systems, mid-circuit measurement and reset (MCMR) operations are performed by scattering light from laser beams and detecting the resulting fluorescence. These dissipative operations typically drive strong atomic transitions with a relatively large spectral bandwidth, where even a single photon from the driving laser or re-radiated light can destroy quantum information stored in nearby data qubits. Isolation can be achieved by using multiple atomic species [7–9], shuttling atoms in and out of measurement/reset zones [10–12], or spatially discriminating auxiliary and data atoms with well-focused laser beams [13]. However, these methods increase the system complexity and can significantly degrade the speed of operations [11].

In this paper, we demonstrate MCMR operations using two different types of qubits in the same atomic species, in a version of the so-called *omg* qubit architecture [14]. Our approach is integrated with a full-stack trapped-ion quantum computing system and allows MCMR operations to be controlled from a high-level software layer and without shuttling, specific spatial ordering of the atoms, or additional individual qubit addressing

optical elements. We note that a similar approach has been demonstrated for neutral atoms [15].

We implement MCMR operations using two different *omg* approaches. The ***hands-off method***[?] does not disturb the data qubits and drives the auxiliary atoms to a metastable qubit state and then cycles them back to the ground state via a short-lived excited state (Fig. 1a). The ***shelving method***[16] shelves the data qubit to metastable states that are isolated from photon scattering, thus nominally protecting the quantum information (Fig. 1b).

Although both methods can achieve high fidelity MCMR, they have different error and speed characteristics. The hands-off method performs all MCMR operations on the auxiliary qubit, thereby limiting exposure of the data qubits to shelving errors. However, this isolation relies on low coupling between the auxiliary drive and the data qubits throughout the measurement or reset sequence. In addition, measurement may be slower, limited by the speed of the auxiliary qubit metastable transition. The shelving method hides the data qubit from the MCMR operations and can provide better crosstalk protection during measurement and reset, but requires high fidelity shelving and high coherence of the metastable state. A comparison between the two methods is therefore a trade-off between the coherence of the shelved state and the unwanted coupling of the metastable state drive and may even depend on whether the subsystem is being measured or just reset, as the measurement requires more photon scattering.

The use of additional metastable states better isolates the data qubit during MCMR operations but requires the added complexity of individual addressing beams to drive specific qubits to the metastable state. This can be accomplished with individual addressing beams already in place for quantum gate operations. Here, the gate beams are exploited to spectrally shift (“dress”) target qubits and a simple global beam is tuned to drive

* Corresponding author: yichao.yu@duke.edu

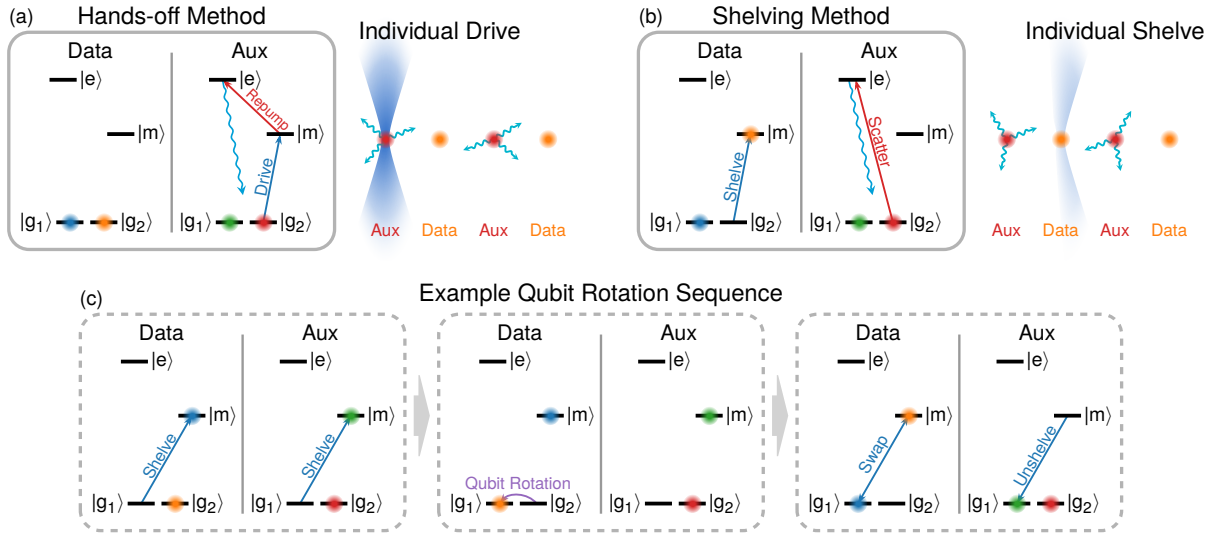


FIG. 1. MCMR sequences via metastable intermediate states. The energy levels here are abstract and may be applicable to different ion types. Most of the qubit operations in circuits are done on the two ground states $|g_1\rangle$ and $|g_2\rangle$. The metastable $|m\rangle$ state has a long enough lifetime such that its decay can be ignored during the sequence. Finally, a short-lived excited state $|e\rangle$ that can be used for photon scattering. Depending on the type of the sequence, different $|e\rangle$ may be chosen for either a cycling or non-cycling transition. (a) The hands-off method does not disturb the data qubit and drives the auxiliary ion to $|m\rangle$ as an intermediate state for photon scattering on $|e\rangle$. (b) The shelving method hides the data qubit in state $|m\rangle$ and measures the auxiliary qubit. (c) Example of the shelving method using a selective pulse sequence. This sequence achieves the same final state as the one in (b) without the need for individual shelving or dressing beams.

only those qubits that have been selected and shifted into resonance with the metastable transition [17]. To best protect the data qubits, the dressing should be applied only to the auxiliary qubits, no matter which *omg* method, hands-off or shelving, is employed. Alternative to dressing, the selective driving of target qubits to the metastable state can be accomplished with single-qubit rotations on the data qubits with the existing individual addressing gate beams and a global shelving beam. An example of such a composite sequence is shown in Fig. 1c. This approach drives all qubits to the metastable state, and is therefore not appropriate for the hands-off *omg* method.

In all, we present three implementations of MCMR operations using the *omg* architecture: the dressing implementation of the hands-off method, the dressing implementation of shelving method, and the qubit rotation implementation of shelving method.

II. EXPERIMENTAL SYSTEM AND CONTROL OF ATOMIC STATES

Here, we demonstrate these methods experimentally using a fully reconfigurable trapped-ion quantum computing system [18]. A chain of $^{171}\text{Yb}^+$ ions is trapped using a Phoenix surface trap fabricated by Sandia National Laboratory [18, 19]. As shown in the level diagram of Fig. 2a, we use the magnetic field insensitive qubit $|1\rangle \equiv |F = 1, m_F = 0\rangle$ and $|0\rangle \equiv$

$|F = 0, m_F = 0\rangle$ in the ground $S_{1/2}$ manifold. The qubit is coherently controlled using 355 nm beams [20] - one global beam addressing all ions in the chain and an array of counter-propagating, tightly-focused beams addressing each ion individually (Fig. 2b). These beams either Stark shift the ground state qubit or drive stimulated Raman transitions between its levels. All other beams used in the experiment are global beams illuminating the entire chain and aligned parallel to the trap surface. Dissipative operations (Doppler cooling as well as the global reset and measurement operations of the qubit states) are done using the 370 nm transition with a state preparation and measurement (SPAM) error of 0.2 % (0.5 %) for the $|0\rangle$ ($|1\rangle$) states. The 935 nm beam is used to repump the ions back to the ground state thus addressing the leakage from $P_{1/2}$ to the metastable $D_{3/2}$. This is achieved with a fixed tone addressing the $D_{3/2}(F = 1)$ hyperfine state, which participates in all of the dissipative operations, and a controllable sideband addressing the $D_{3/2}(F = 2)$ hyperfine state that is switched on during cooling and pumping and can be switched off during detection.

We use the metastable $D_{3/2}$ states to implement MCMR in the *omg* architecture coherently controlled by a 435 nm beam (Fig. 2b). Since the $D_{3/2}(F = 1)$ state is continuously driven by the fixed 935 nm tone, we only use the 435 nm beam to drive the ion to the $D_{3/2}(F = 2)$ state. Depending on the lock point, we are able to drive either the $F = 1$ or $F = 0$ hyperfine levels in the $S_{1/2}$ manifold to the $D_{3/2}$ state. Due to off-resonant scattering from the fixed 935 nm tone, the lifetime of

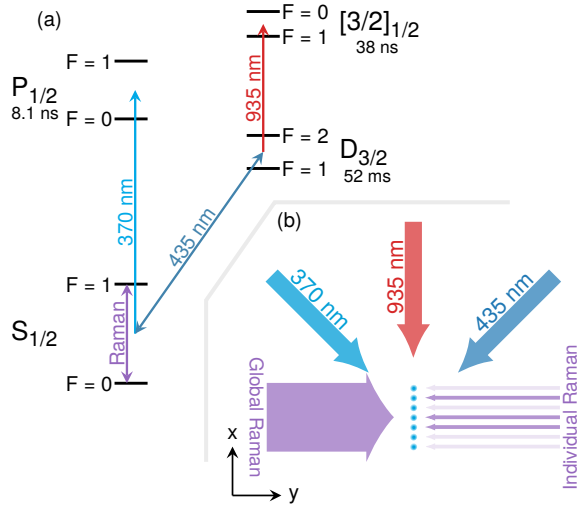


FIG. 2. Overview of the experiment. (a) Relevant energy levels and supported operations on the $^{171}\text{Yb}^+$ ions. The normal reset and measurement operation is done on the 370 nm transition between $S_{1/2}$ and $P_{1/2}$ with population leakage into the $D_{3/2}$ repumped back with the 935 nm transition via the $[3/2]_{1/2}$ state. The metastable $D_{3/2}$ state can also be directly populated using the 435 nm transition. (b) Beam geometry relative to the ion chain. The 370 nm and 435 nm beams are sent in 45° relative to the ion chain parallel to the trap surface and the 935 nm beam is sent in along the chain. All of these are global beams that illuminate the whole chain. The Raman beam path consists of a global beam perpendicular to the chain and an array of counter-propagating individual beams to target each ion separately.

the $D_{3/2}(F=2)$ state is shortened to 15 ms from the 53 ms natural lifetime. We also measured a T_2 coherence time of 10 ms. These technical issues limit the fidelity of our MCMR sequence and could be improved with better control on the 935 nm beam and better locking of the 435 nm laser.

The dressing implementation for achieving individual control during the MCMR sequence requires the use of the individual Raman beams to dress the auxiliary ion and change the resonance of the 435 nm transition. However, the wavelength of Raman beams used in our system is selected to minimize the scalar AC Stark shift on the $S_{1/2}$ state in order to improve gate fidelity caused by the differential Stark shift during gate operations. Additionally, the Raman light is far detuned from any D state transitions, and therefore we cannot produce a significant shift on the shelving transition by simply turning on the individual Raman beams. Instead, we rely on dressing the ions with a Raman transition. The Hamiltonian of an ion driven on a Raman transition with a Raman Rabi frequency of Ω and a detuning of δ can be written as:

$$H = \delta|0\rangle\langle 0| + \frac{\Omega}{2}(|0\rangle\langle 1| + |1\rangle\langle 0|) \quad (1)$$

This produces two dressed states

$$|\psi_{\pm}\rangle = \frac{\sqrt{1 \pm \delta/\Omega_g}|0\rangle \pm \sqrt{1 \mp \delta/\Omega_g}|1\rangle}{\sqrt{2}} \quad (2)$$

with corresponding frequency shifts from the bare resonance,

$$\Delta_{\pm} = \frac{\delta \pm \Omega_g}{2} \quad (3)$$

where $\Omega_g \equiv \sqrt{\Omega^2 + \delta^2}$ is the generalized Rabi frequency. The two dressed states are shifted from the bare resonance with opposite signs, and the absolute values of the shifts are different when $\delta \neq 0$. The one with a smaller shift is usually called the Stark shifted state whereas the resonance with a larger shift corresponds to a multi-photon transition. This asymmetry gives rise to different requirements for the dressing beam when it is used in the direct or shelving methods. For the hands-off method, where the dressed auxiliary ions are driven to the metastable state, only the dressed state needs to be sufficiently shifted to avoid driving the data ions, this allows a larger shift asymmetry, i.e. a large δ , to be used. In contrast, the shelving method drives the data ions to the metastable state while leaving both dressed states untouched for the auxiliary ions, therefore favoring a more symmetric shift and a smaller δ . Moreover, in order to reduce the effect of crosstalk from the dressing beam on the data ions, δ should not be zero even for the shelving method and should be significantly larger than the crosstalk Raman Rabi frequency.

Apart from the considerations during the drive to the metastable state when the ions are dressed, the process of mapping the two qubit states to and from the two dressed states accurately and robustly on the auxiliary ion is also important for achieving a high MCMR fidelity. Although the qubit phase and the exact quantum state are not maintained during a measurement or a reset, the dressing and shelving sequence still needs to maintain the population in the two qubit states upon entering a measurement and when exiting a reset operation. While this could be achieved by adiabatically turning on the dressing beam, such a process is generally slow, especially when the detuning is comparable to or smaller than the Rabi frequency.

Instead, we use a single qubit rotation to map between the two bases. The target unitary itself depends on the power of the Raman beams, $U(\Omega) = |\psi^+\rangle\langle 0| + |\psi^-\rangle\langle 1| + h.c.$. We therefore use numerical optimization to construct a composite pulse that is robust for a range of Rabi frequencies around the nominal value. Additionally, the sequence also rotates the neighboring ions into the dressed states for low Rabi frequencies. This ensures that the error accumulated from the crosstalk from the Raman beams would be predominantly a phase error and can be corrected with spin echo pulses during the MCMR sequence. Table I lists the sequence parameters designed for different nominal detuning values and their

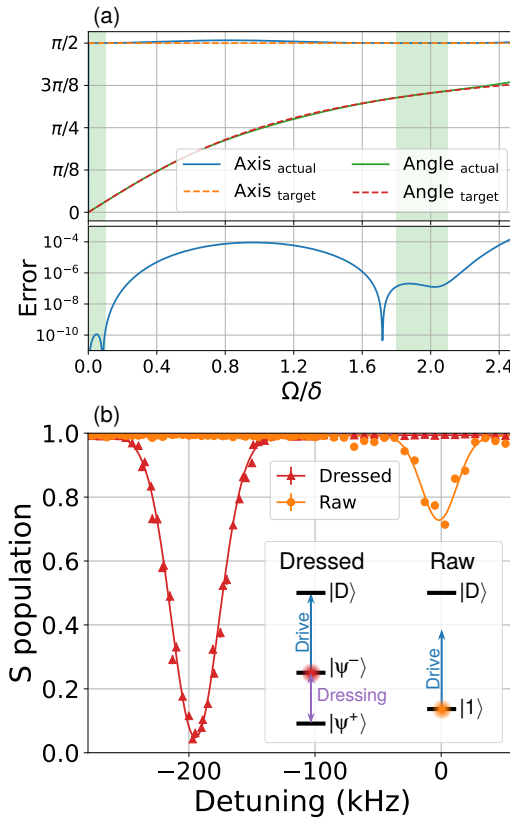


FIG. 3. Individual shelving to the $D_{3/2}$ state by Raman dressing. (a) Performance of an example rotation sequence between the undressed and dressed state for $\delta/\Omega = 0.5$. The rotation axis, angles (upper) and the error of the rotation (lower) is plotted as a function of the Rabi frequency. The green band marks the relevant range of Rabi frequency. (b) Simultaneous $D_{3/2}$ spectrum on two ions with individual dressing on one ion. Inset: illustration of the measurement protocol.

performance. As an example, Fig. 3a plots the calculated rotation performed by the pulse sequence for $\delta/\Omega = 0.5$ and the error it produces from the expected one, showing an expected error of no more than 10^{-6} in the relevant range of Rabi frequencies.

We demonstrate the individual shelving capability by measuring the D state spectrum on two ions simultaneously. One ion is prepared in the $|\psi^-\rangle$ dressed state with the robust pulse sequence, whereas the other ion is not dressed and remains in $|1\rangle$ (Fig. 3b). We drive the ions to the D state using a Blackman time profile to suppress off-resonant excitation [21]. The pulse length is chosen to drive a π rotation for the dressed state and is the same for both measurements to allow easier comparison. This pulse length causes the more strongly coupled bare resonance to be overdriven and combined with the Blackman pulse shape gives rise to a smaller peak height.

| | | Sequence 1 | Sequence 2 |
|---------|-------------------|-----------------------|----------------------|
| Target | δ/Ω | 0.1 | 0.5 |
| | δ_1/Ω | 0.066045984 | 0.865404511 |
| | $\tau_1\Omega$ | 6.101 | 2.482 |
| | ϕ_1 | 4.697118972032 | 5.922001257829 |
| Pulse 1 | δ_2/Ω | 1.738387469 | -0.467035375 |
| | $\tau_2\Omega$ | 3.372 | 5.03 |
| | ϕ_2 | 0.0 | 3.710143207203 |
| Pulse 2 | δ_3/Ω | -0.304962921 | 0.087101714 |
| | $\tau_3\Omega$ | 7.47 | 4.478 |
| | ϕ_3 | 2.106261199596 | 0.56914785185 |
| Errors | E_0 | 2.5×10^{-4} | 2.9×10^{-7} |
| | E_1 | 1.9×10^{-10} | 2.3×10^{-7} |

TABLE I. Rotation sequence parameters and performance. Each of the composite pulse sequence contains three Raman pulses with detuning δ_i , time τ_i and ϕ_i ($i = 1, 2, 3$). The detunings and times are recorded in the table as unitless number relative to the nominal Rabi frequency Ω . E_0 is the total error in the Pauli X and Y coefficient for a crosstalk Rabi frequency of 0 to 5 % of the nominal Rabi frequency, and E_1 is the error for a fluctuating target ion Rabi frequency from 90 % to 105 % of nominal. The significant digits recorded in the table reflects the hardware resolution used in our experiment.

III. MCMR EXPERIMENTS AND RESULTS

For the demonstrations of MCMR, we use two ions separated by $4.5 \mu\text{m}$, which is the same as the distance used for gate operations. Due to several technical reasons, we cannot detect the emitted 297 nm photons ($D[3/2]_{1/2} \rightarrow S_{1/2}$ transition). We instead, use the shelving method (Fig. 1b) for mid-circuit measurement, combined with the hands-off method (Fig. 1a) for mid-circuit reset. This limitation could be overcome in the future with the addition of a $2.438 \mu\text{m}$ laser to pump the $D_{3/2}$ state back via the $P_{1/2}$ state, emitting a 370 nm photon that we could detect[22].

A. Mid-circuit measurement

We show mid-circuit measurement using the shelving method (Fig. 4a) with both the dressing and the qubit rotation implementations to distinguish between the data and the auxiliary ions. In both cases, the ion chain is cooled to the motional ground state on all three axes. Since the destination of the auxiliary $|0\rangle$ state will not affect the measurement result as long as it is not in $|1\rangle$, the sequence for both implementations can be significantly simplified. The $|1\rangle$ state of the auxiliary ion is untouched.

In the case of the dressing implementation, the shelving sequence first dresses the auxiliary ions with the Raman beams and drives only the data ion's $|0\rangle$ state to $|D\rangle \equiv |D_{3/2}, F = 2, m_F = 0\rangle$. The dressing is done with a detuning of $\delta = 0.1\Omega$ and uses the corresponding sequence in Table I for rotating in and out of the dressed

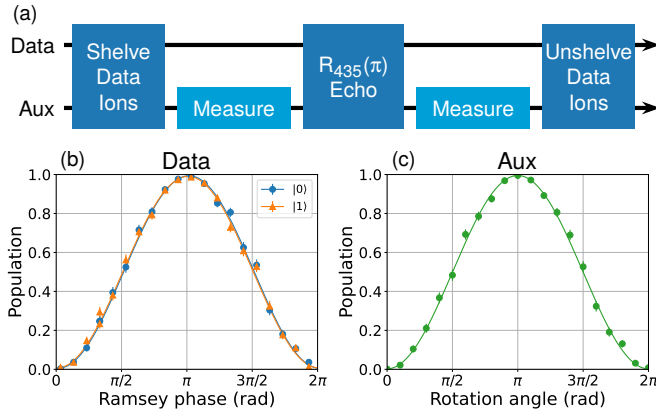


FIG. 4. Mid-circuit measurement with shelving method (Fig. 1b) to the $D_{3/2}$ manifold. (a) Experimental sequence. First, the data ions are shelved to the $|D\rangle$ state. The auxiliary ion is measured using the 370 nm transition with a pause for the global spin echo to improve data ion fidelity. After the measurement, the data ions are unshelved back to the ground states. The shelving and unshelving of the data ions may use either the dressing implementation or a simplified qubit rotation sequence. (b) Ramsey phase scan demonstrating that the mid-circuit measurement of the auxiliary ion using the qubit rotation implementation preserves the coherence of the data ion coherence. The contrast of the Ramsey fringe shows a data ion fidelity of 98.8(6) % (98.2(7) %) when the auxiliary ion was in the $|0\rangle$ ($|1\rangle$) state. (c) Mid-circuit measurement on the auxiliary ion which is initialized in a superposition of $|0\rangle$ and $|1\rangle$ with a single qubit rotation $R_x(\theta)$ with variable rotation angle θ . The result shows a measurement fidelity of 99.6(2) % which is identical to that of a normal measurement.

states. After this, the data ion's $|1\rangle$ state is driven to $|0\rangle$ using our typical Raman transition. The final mapping is: $|0\rangle \rightarrow |D\rangle$, $|1\rangle \rightarrow |0\rangle$ on the data ions, and no operation on the auxiliary ions.

For the qubit rotation implementation, the shelving sequence uses a global drive from $|0\rangle$ to $|D\rangle$ followed by the same Raman step to transfer the data ion's $|1\rangle$ to $|0\rangle$. The mapping is: $|0\rangle \rightarrow |D\rangle$, $|1\rangle \rightarrow |0\rangle$ on the data ions, and $|0\rangle \rightarrow |D\rangle$ on the auxiliary ions. Note that with this simplification, the dressing sequence is strictly more complex than the qubit rotation one since it requires additional Raman dressing during the drive to the $|D\rangle$ state. However, this simplification relies on the $F = 1$ and $F = 0$ ground state hyperfine structure, which allows the data qubit to remain in $|0\rangle$ during measurement, and does not apply to all ions, e.g. $^{137}\text{Ba}^+$, where the dressing implementation may be preferred.

After the shelving step, the detection of the auxiliary ions then proceeds to the 370 nm transition. We use a π pulse between $|0\rangle$ and $|D\rangle$ in the middle of the detection time to perform spin echo on the data ion. This echo is done with the global 435 nm beam, but it does not affect the measurement result on the auxiliary ion, since it is not coupled to the $|1\rangle$ state. Finally, we apply the inverse

of the shelving sequence to bring the data ion back to the $|0\rangle$ and $|1\rangle$ states. The shelving and unshelving process each takes 26 μs (47 μs) for the qubit rotation (dressing) implementation, and the photon scattering step takes 140 μs .

We characterize the fidelity of the mid-circuit measurement for the auxiliary ion in both the $|0\rangle$ and $|1\rangle$ states by performing a single qubit rotation on the auxiliary ion before the entire measurement sequence is applied (Fig. 4c). We show a measurement fidelity of the $|0\rangle$ ($|1\rangle$) state of 99.7(1) % (99.5(3) %) regardless of the shelving implementation. This result is indistinguishable from the end-of-circuit measurement fidelity in our setup. In addition, the effect of the auxiliary ion measurement sequence on the data ion was measured via a Ramsey experiment. For the qubit rotation implementation, the data ion fidelity extracted from the Ramsey fringe in Fig. 4b is 98.8(6) % (98.2(7) %) when the auxiliary ion was in $|0\rangle$ ($|1\rangle$) state. The fidelity is limited by the coherence of the $S_{1/2} \rightarrow D_{3/2}$ transition as discussed in section II. For the dressing implementation, the data qubit fidelity is 91.7(4) % when the auxiliary ion is in either $|0\rangle$ or $|1\rangle$. The low fidelity of this implementation is due to crosstalk from the Raman dressing beams, as expected. It could be improved by changing the dressing parameters, e.g. increasing the dressing detuning. However, we do not optimize this method further due to its intrinsic disadvantage on our system compared to the qubit rotation implementation. The fidelities of the data qubit for both implementations are SPAM corrected.

B. Mid-circuit reset

We perform mid-circuit reset using the dressing implementation of the hands-off method. The dressing is done with $\delta/\Omega = 0.5$. The corresponding sequence in Table I is used to rotate in and out of the dressed states. In order to fully reset the ion to a single state, we also need to pump $|2\rangle \equiv |F = 1, m_F = -1\rangle$ and $|3\rangle \equiv |F = 1, m_F = 1\rangle$ that are outside the qubit space. We drive these states to the $|D_{3/2}, F = 2, m_F = -1\rangle$ and $|D_{3/2}, F = 2, m_F = 1\rangle$ respectively using a 435 nm global beam. These transitions are isolated by a sufficient Zeeman shift (5 MHz) from any transitions on the states populated by the data ion (Fig. 5a). After driving the desired auxiliary ion states to $D_{3/2}$, we use 935 nm light to pump $D_{3/2}$ states back to $S_{1/2}$ to complete a pumping cycle. We perform the reset with different numbers of pumping cycles. Fig. 5c shows the pumping error measured on the auxiliary ion starting with either the $|0\rangle$ or $|1\rangle$ initial states. 16 pumping cycles is sufficient to complete the auxiliary qubit reset operation with a 0.9(3) % error. Fig. 5b shows the error on the data ion during the pumping process with 3.7(5) % error after 16 cycles. The infidelity is mainly caused by off-resonant coupling to the $D_{3/2}$ state and

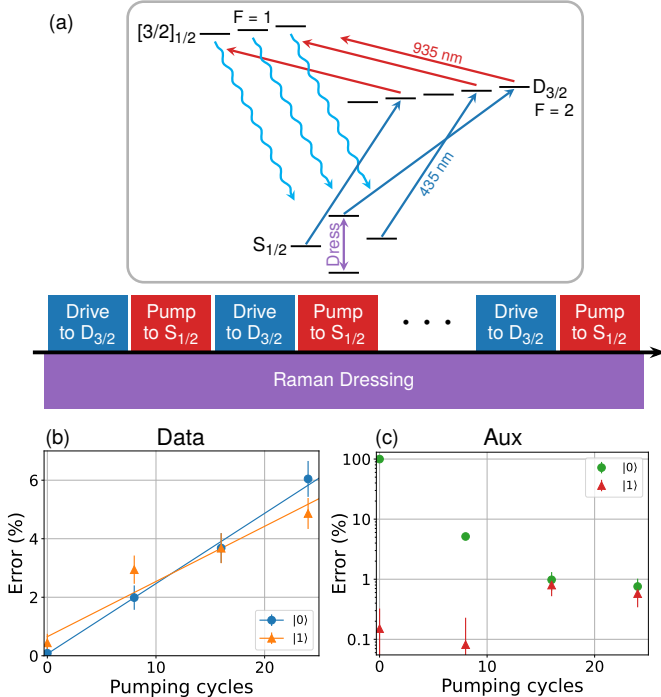


FIG. 5. Mid-circuit reset with hands-off method (Fig. 1a) using the $D_{3/2}$ manifold. (a) Experimental sequence. The auxiliary ion is dressed with the Raman beams during the whole sequence. The population in the undesired states ($|0'\rangle$, $|2\rangle$ and $|3\rangle$) are driven to the $D_{3/2}$ states by 435 nm light and then pumped back down to the $S_{1/2}$ states by 935 nm. This process repeats until all the population is pumped to the $|1'\rangle$. (b, c) Infidelity of the data ion and the auxiliary ion after pumping, demonstrating a 0.9(3) % error on auxiliary ion and 3.7(5) % on data ion after 16 cycles of pumping.

the motional excitation of the ions. Due to technical limitations, the ions are not cooled to the ground motional state for this reset demonstration. The fidelity on both the data and auxiliary ions are SPAM corrected.

IV. SUMMARY AND OUTLOOK

We studied how *omg* architecture can be used for MCMR in a trapped-ion quantum computing system with long chains of ions. These methods provide a speedup by avoiding the time-consuming shuttling and re-cooling steps without the need for additional individually addressed beams. We experimentally demonstrated all three of these implementations on our $^{171}\text{Yb}^+$ quantum computing system without any additions to our existing setup. Ultimately, the choice of which MCMR method to use for a particular system depends on a number of factors, notably the coherence of the metastable state, the fidelity of ground state qubit operations, the available optical power, and the detector used to measure the photons scattered from the ions.

The fidelity achieved is limited mainly by technical sources and can be straightforwardly improved with better laser locking, laser power and polarization control, and performing ground state cooling on the ion chain. Switching to a metastable state with longer lifetime, e.g. $F_{7/2}$ for Yb^+ or $D_{3/2}$ and $D_{5/2}$ for Ba^+ , could also improve the fidelity significantly.

While the photon scattering during measurement causes recoil heating, it is negligible for reset, which only requires few photons to be scattered. Furthermore, heating during measurement can be minimized by integrating EIT [23] or sideband cooling [24] into the detection process.

V. ACKNOWLEDGMENTS

This work is supported by the DARPA Measurement-based Quantum Information and Transduction program (HR0011-24-9-0357), the DOE Quantum Systems Accelerator (DE-FOA-0002253), the NSF STAQ Program (PHY-1818914), and the NSF Major Research Instrumentation program (2117530).

[1] Y. Alexeev *et al.*, *PRX Quantum* **2**, 017001 (2021).
[2] E. Altman *et al.*, *PRX Quantum* **2**, 017003 (2021).
[3] D. Awschalom *et al.*, *PRX Quantum* **2**, 017002 (2021).
[4] J. Ye and P. Zoller, *Phys. Rev. Lett.* **132**, 190001 (2024).
[5] S. Majumder, L. Andreata de Castro, and K. R. Brown, *npj Quantum Information* **6**, 19 (2020).
[6] J. R. and, *Contemporary Physics* **60**, 226 (2019).
[7] P. O. Schmidt, T. Rosenband, C. Langer, W. M. Itano, J. C. Bergquist, and D. J. Wineland, *Science* **309**, 749 (2005).
[8] J. M. Pino, J. M. Dreiling, C. Figgatt, J. P. Gaebler, S. A. Moses, M. Allman, C. Baldwin, M. Foss-Feig, D. Hayes, K. Mayer, *et al.*, *Nature* **592**, 209 (2021).
[9] K. Singh, C. E. Bradley, S. Anand, V. Ramesh, R. White, and H. Bernien, *Science* **380**, 1265 (2023).
[10] D. Zhu, G. D. Kahanamoku-Meyer, L. Lewis, C. Noel, O. Katz, B. Harraz, Q. Wang, A. Risinger, L. Feng, D. Biswas, L. Egan, A. Gheorghiu, Y. Nam, T. Vidick, U. Vazirani, N. Y. Yao, M. Cetina, and C. Monroe, *Nature Physics* **19**, 1 (2023).
[11] S. A. Moses *et al.*, *Physical Review X* **13**, 041052 (2023).
[12] D. Bluvstein, H. Levine, G. Semeghini, T. T. Wang, S. Ebadi, M. Kalinowski, A. Keesling, N. Maskara, H. Pichler, M. Greiner, V. Vuletić, and M. D. Lukin, *Nature* **604**, 451 (2022).

[13] S. Motlakunta, N. Kotibhaskar, C.-Y. Shih, A. Vogliano, D. McLaren, L. Hahn, J. Zhu, R. Hablützel, and R. Islam, *Nature Communications* **15**, 6575 (2024).

[14] D. T. C. Allcock, W. C. Campbell, J. Chiaverini, I. L. Chuang, E. R. Hudson, I. D. Moore, A. Ransford, C. Roman, J. M. Sage, and D. J. Wineland, *Applied Physics Letters* **119**, 214002 (2021).

[15] J. W. Lis, A. Senoo, W. F. McGrew, F. Rönchen, A. Jenkins, and A. M. Kaufman, *Physical Review X* **13**, 10.1103/PhysRevX.13.041035 (2023).

[16] T. Manovitz, Y. Shapira, L. Gazit, N. Akerman, and R. Ozeri, *PRX Quantum* **3**, 010347 (2022).

[17] Jamie D Leppard, Ana S Sotirova, Andres Vazquez-Brennan, Sophie M Decoppet, David P Nadlinger, Fabian Pokorny, and Chris J Ballance, in *Bulletin of the American Physical Society* (American Physical Society, Fort Worth, Texas, 2024).

[18] A. Kozhanov, Y. Yu, L. Zhukas, L. Feng, D. Biswas, B. Harraz, K. Yan, V. Zhang, C. Noel, and C. Monroe, in *Optica Quantum 2.0 Conference and Exhibition (2023), Paper QM3A.2* (Optica Publishing Group, 2023) p. QM3A.2.

[19] M. C. Revelle, ArXiV (2020), [arXiv:2009.02398](https://arxiv.org/abs/2009.02398).

[20] M. Cetina, L. Egan, C. Noel, M. Goldman, D. Biswas, A. Risinger, D. Zhu, and C. Monroe, *PRX Quantum* **3**, 010334 (2022).

[21] Blackman, R. B. and Tukey, J. W, in *The Measurement of Power Spectra. From the Point of View of Communications Engineering* (Dover Publ, New York, 1958) pp. 98–99.

[22] A. Kramida and Y. Ralchenko, *NIST Atomic Spectra Database, NIST Standard Reference Database 78* (1999).

[23] K. N. Blodgett, D. Peana, S. S. Phatak, L. M. Terry, M. P. Montes, and J. D. Hood, *Physical Review Letters* **131**, 083001 (2023), [arXiv:2305.02405 \[physics\]](https://arxiv.org/abs/2305.02405).

[24] M. F. Parsons, F. Huber, A. Mazurenko, C. S. Chiu, W. Setiawan, K. Wooley-Brown, S. Blatt, and M. Greiner, *Physical Review Letters* **114**, 213002 (2015).